

Deformational Features and Microstructure Evolution of Copper Fabricated by a Single Pass of the Elliptical Cross-Section Spiral Equal-Channel Extrusion (ECSEE) Process

Chengpeng Wang, Fuguo Li, and Juncheng Liu

(Submitted September 3, 2017; in revised form January 29, 2018; published online April 18, 2018)

The objectives of this work are to study the deformational feature, textures, microstructures, and dislocation configurations of ultrafine-grained copper processed by the process of elliptical cross-section spiral equal-channel extrusion (ECSEE). The deformation patterns of simple shear and pure shear in the ECSEE process were evaluated with the analytical method of geometric strain. The influence of the main technical parameters of ECSEE die on the effective strain distribution on the surface of ECSEE-fabricated samples was examined by the finite element simulation. The high friction factor could improve the effective strain accumulation of material deformation. Moreover, the pure copper sample fabricated by ECSEE ion shows a strong rotated cube shear texture. The refining mechanism of the dislocation deformation is dominant in copper processed by a single pass of ECSEE. The inhomogeneity of the micro-hardness distribution on the longitudinal section of the ECSEE-fabricated sample is consistent with the strain and microstructure distribution features.

Keywords copper, extrusion, hardness, microstructure, severe plastic deformation, ultrafine grain

1. Introduction

It is known to all that the grain refinement of metallic material can be achieved by traditional plastic processing methods such as cold rolling, cold drawing, and upsetting. However, the ultrafine-grained (UFG) materials produced by these methods always appear the low-angle grain boundaries of non-equilibrium (LAGBs), different from steady high-angle grain boundaries (HAGBs) (Ref 1). A far cry from the traditional methods, severe plastic deformation (SPD) gives a special approach to the refinement of coarse grains under the three-direction pressure state of intense plastic deformation. Recently, SPD has been extensively used in the fabrication of various UFG materials, including metal, alloys, polymers, and even composite materials (Ref 2). However, SPD microstructure evolution and grain refinement mechanisms are still quite complicated (Ref 3). Therefore, further systematic research on the SPD refinement mechanism is indispensable to improve the

SPD preparation methods of various bulk micro/nano-materials.

The combined deformation mode of compression and torsion is regarded as an effective method of UFG material fabrication. With the elliptical cross-section spiral equal-channel extrusion (ECSEE) proposed recently as a relatively novel method, ECSEE efficiency in material formation is ascribed to the joint deformation of torsion shear, extrusion, and upsetting (Ref 5). Recently, ECSEE has been successfully used for preparing UFG copper (Ref 4-6) and aluminum alloy (Ref 7). Wang et al. (Ref 4, 5) studied numerically and experimentally pure copper processed by a single pass of ECSEE. The effective strain on the transverse section of the ECSEE-processed samples was analyzed by the finite element simulation. The experiments were performed to access the grain refinement and hardness distribution by means of metallograph observation and micro-hardness measurement, respectively. Li et al. (Ref 6, 7) compared the deformation modes of ECAP, ECSEE, and torsion and classified these into the combined bending-torsion, combined tension-torsion, and pure shear. The authors consider that such a classified method is less rigorous for the forming mode. Moreover, Li's study focused on the micro-hardness distribution and microstructural evolution of pure Al during ECSEE. As far as the industrial application is concerned, the structural parameters of ECSEE die were optimized by the grey theory (Ref 8). The simplified slice-plain-strain method and incorporation of the incremental superposition theory were utilized for calculating the effective strain accumulation from ECSEE (Ref 9). The fabrication of UFG materials is indispensable to both academic and industrial points of view. However, there have been fewer systematic researches of the microstructural evolution and grain refinement mechanism for UFG materials fabricated by means of the ECSEE.

Chengpeng Wang, School of Materials Science and Engineering, Tianjin Polytechnic University, Tianjin 300387, People's Republic of China; and College of Materials Science and Engineering, Taiyuan University of Technology, Taiyuan 030024, People's Republic of China; **Fuguo Li**, School of Materials Science and Engineering, Northwestern Polytechnical University, Xi'an 710072, People's Republic of China; and **Juncheng Liu**, School of Materials Science and Engineering, Tianjin Polytechnic University, Tianjin 300387, People's Republic of China. Contact e-mails: cpwang2003@foxmail.com, fuguolx@nwpu.edu.cn, and jchliu@tjpu.edu.cn.

In the current studies of high-pressure torsion (HPT) and torsion extrusion (TE), the crossover and multiplication of dislocations easily impacted the shear zone of the material. The cell body of the microstructure can transform into the grain structure. The material grain refinement is finally achieved under the torsional shear deformation mode (Ref 10). Nevertheless, the equiaxed grain and HAGB formation mechanisms in the SPD-induced materials are not well comprehended by virtue of the complexity of microstructure evolution, in that ECSEE has the inclination to be a relatively new SPD method, and ECSEE-related research is still during its course of exploration. It is vital to understand the grain refinement mechanism of the material during the process of ECSEE. Notwithstanding, systematic investigations on the microstructure evolution and grain refinement mechanism are anything more than sufficient. This study aims to experimentally examine a single pass of ECSEE of pure copper by means of theory, simulation, and experiment.

2. ECSEE Principle

2.1 Simple Shear Model in ECSEE

As the schematic diagram of ECSEE is illustrated in Fig. 1(a), the channel of the ECSEE die consists of three parts: Channel L_1 , Channel L_2 , and Channel L_3 . The round-bar sample is extruded through the cross-section changes of round ellipse, elliptical cross-sectional torsion, and ellipse round via the above channels of the ECSEE die (Ref 4, 5). The ECSEE-induced sample undergoes severe deformation while maintaining its initial cross section. Under this circumstance, the sample is allowed to be extruded repeatedly, causing deformation accumulation for the material grain refinement (Ref 5).

Shear deformation plays a significant role in the SPD refinement of materials (Ref 11). Intensive shear deformation is also executed in the course of ECSEE. The plane deformations of pure shear and simple shear are shown in Fig. 1(b) and (c), respectively. By and large, pure shear exists in the traditional tension and compression deformation. The effect of Channel L_1 and Channel L_3 is considered as the tension–compression mode, and thus pure shear is generated more in these two channels. The directions of the principal strain axes x and y do not rotate and change with the progressive strain of pure shear (see Fig. 1(b)). Hence, pure shear deformation is also called non-rotational deformation or coaxial deformation. By contrast, the length of the two principal strain lines could continually elongate or shorten, respectively. With the exception of the principal strain line, the direction and length of all direction lines regularly change during the progressive deformation. Simple shear is mainly considered to exist in Channel L_2 for the torsion deformation mode. We note that the pure shear and simple shear do not have an obvious demarcation in the actual deformation process, and they can be transformed from one into the other. The directions of the strain axes x and y could rotate in the progressive process of simple shear (see Fig. 1(c)). Therefore, the simple shear deformation is known as rotational deformation or non-coaxial deformation, in contrast to its pure shear counterpart. The symbol N denotes the direction of the shear plane in Fig. 1(c). With the exception of the parallel shear plane direction lines, all directions and lengths of direction lines could change with the progressive deformation. Simple shear

deformation consists of a series of parallel sliding layers formed by shear slip.

2.2 Geometric Analysis of Effective Strain

In view of the significance of the ECSEE Channel L_2 , the elliptical cross section is approximately simplified into a round cross section. Deformation flow of the ECSEE-induced material appeared along the space spiral curve during the plastic deformation (indicated in Fig. 2). The spiral track of ECSEE deformation is designated in the Cartesian coordinates x – y – z . The marked point on the x – y plane and a unit cell (blue block in the figure) are selected as the research object. The amplifier unit cell as the study focus of the micro-torsion of torsional angle $d\varphi$ is depicted in Fig. 2(b). The initial unit cell ABCD–EFGH transforms into the oblique prism A'B'CD–E'F'GH under the driving of simple shear. Shear angles α and β are initiated by the constructive change of the unit cell. As far as we can see, the angle α is greater than β due to the torsion characteristic (in Fig. 2(b)). The different stress and strain distributions in the central and peripheral positions on the cross section of ECSEE-induced sample can be unambiguously observed. Previous studies have verified the non-uniformity of deformation in ECSEE (Ref 4, 5).

To investigate the influence factors of ECSEE strain, geometric analysis was adopted with the simplified model of a round cross section instead of the elliptic cross section. As it is indicated in Fig. 2(b) and (c), the rectangle ABCD transforms into the parallelogram A'B'CD under the application of shear deformation. Assuming the coordinates of point A (x_1, z_1), and point A' (x_2, z_2),

$$Z_2 = Z_1, \quad x_2 = x_1 + z_1 c \tan \alpha \quad (\text{Eq 1})$$

As shown in Fig. 2(d), the geometric relationship is given by

$$c \tan \alpha = \tan(90^\circ - \alpha) = \frac{AA'}{AD} \approx \frac{AA''}{AD} = \frac{d\varphi D_1}{2z_1}, \quad (\text{Eq 2})$$

where D_1 is the diameter of the as-received sample or the die channel. Therefore, the expression for the strain can be obtained as (see Fig. 2(c))

$$\varepsilon = \ln \frac{DB'}{DB} = \ln \frac{\sqrt{x_1^2 + z_1^2 c \tan^2 \alpha + z_1^2}}{\sqrt{x_1^2 + z_1^2}} \quad (\text{Eq 3})$$

Using formulas (1) and (2), we can obtain

$$\varepsilon = \ln \frac{DB'}{DB} = \frac{1}{2} \ln \left(1 + \frac{(d\varphi D_1)^2}{4(x_1^2 + z_1^2)} \right) = \frac{1}{2} \ln \left(1 + \frac{d^2 \varphi \sin^2 \psi}{4} \right), \quad (\text{Eq 4})$$

where ψ is the angle between the line of an arbitrary point and the center point and the central axis.

As it can be seen from the above formulas, the strain value of an arbitrary point on the assumed round cross section of ECSEE-induced sample is associated with the angles ψ and $d\varphi$. Essentially, the angle ψ decides the distance from the point to the center of entrance section. When the diameter of the cylindrical sample is determined, the length parameters of Channel L_2 act a decisive role in the torsion shear deformation (Ref 2, 4, 5). Additionally, the ratio of the major-axis and minor-axis lengths m is also associated with the elliptical section. In previous investigations, the strain distribution of the elliptical section differed from that of the conventional round section of as-formed billet (Ref 4, 5). As it is shown in

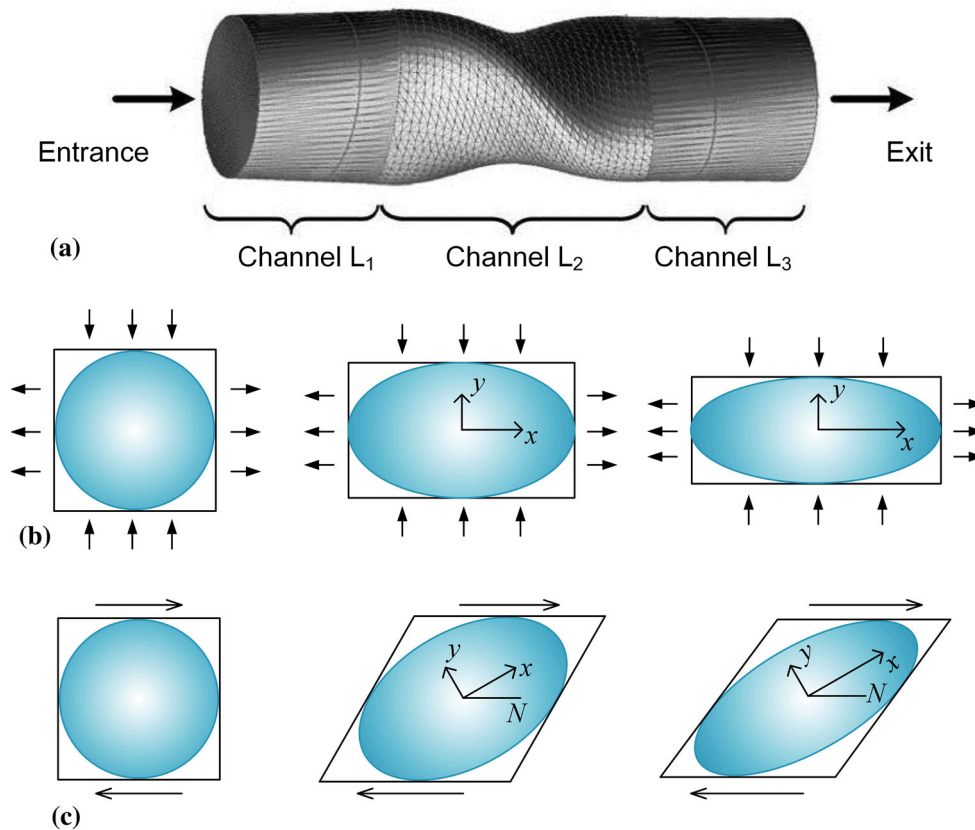


Fig. 1 Schematic diagram of (a) the ECSEE principle, (b) pure shear deformation, and (c) simple shear deformation

Fig. 2(e), the cross-sectional area can be divided into I-reinforced region (red-filled), II-disappearing region (blue slash-filled), and III-normal region (green-filled). Compared to the round cross section, Region I represents a strong torsional torque. As far as the strain value of points on the cross-section boundary is concerned, the maximum value is obtained at the point *N* and the minimum at the point *M* with ignoring the point in the central area.

The strain value of an arbitrary point, as shown in formula (4), is also multiplied by the coefficient related to the variable *m* greater than 1. The coefficient μm takes into account that the area is oval shaped.

$$\varepsilon = \frac{\mu m}{2} \ln \left(1 + \frac{d^2 \varphi \sin^2 \psi}{4} \right), \quad (\text{Eq 5})$$

where μ is a variable coefficient related to the intrinsic properties of deformation materials such as the hardening index, crystalline structure, and alloy phase.

In conclusion, the strain value is strongly concerned with the L_2 , φ , and *m* parameters. Properly speaking, the torsional angle of unit length and the ratio *m* are prone to be the decisive parameters for the ECSEE strain accumulation.

3. Numerical and Experimental Procedures

3.1 ECSEE Evaluation Parameters

The structure parameters of the ECSEE die involve the length of Channel L_2 , the torsional angle φ , the ratio *m*, and the

diameter D_1 of Channel L_1 . In the process of die design, the diameter of round-bar sample is fixed. The matching deformation degree is decided by changing the main structural parameters of the ECSEE die. For the design of the die structure, the diameter D_1 and length of Channel L_2 are basically set. Only the value of the torsional angle φ must be optimized. This can be attributed to important parameters, namely the per unit length of the torsional angle. Therefore, only the examination of different torsional angles can be carried out in the following design analysis. The selection of an appropriate value of *m* is of great importance. This parameter is key to the ECSEE process design. If the value of *m* were much too large, the ellipse would not be transformed back to a round shape for the cold extrusion forming. If the value were much too small, the deformation efficiency would be reduced. Moreover, the contact friction factor of die, *k*, is cardinal to the shear strain. Therefore, the friction factor *k*, torsional angle φ , and ratio *m* were picked out as the design objects.

3.2 Finite Element Method

The simulation software DEFORM 3D v6.1 was used for the reliability evaluation of the ECSEE technique (see Fig. 3(a)). The diameter and length of the as-deformed pure copper sample are 10 mm and 35 mm, respectively. The related parameters of ECSEE die were set as follows: (1) $k = 0.008, 0.2, 0.3, 0.5, 0.7$ for $\varphi = 90^\circ, m = 1.5$; (2) $\varphi = 30^\circ, 45^\circ, 60^\circ, 75^\circ, 90^\circ$ for $k = 0.1, m = 1.5$; and (3) $m = 1.1, 1.2, 1.3, 1.4, 1.5$ for $k = 0.1, \varphi = 90^\circ$. The structure parameters of the ECSEE die are as follows: $L_1 = 7$ mm, $L_2 = 10$ mm, and $L_3 = 7$ mm.

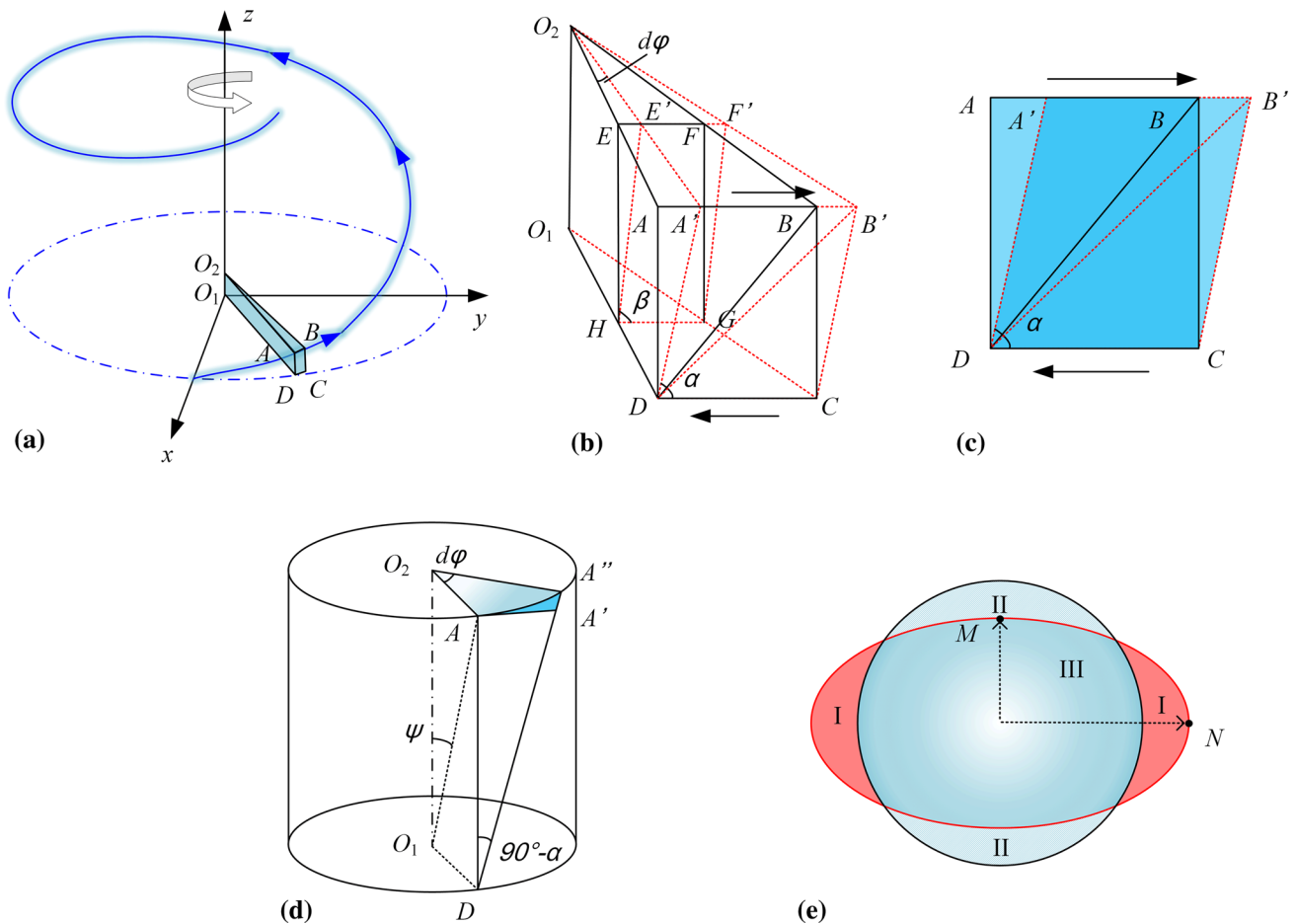


Fig. 2 Shear deformation of a unit cell in ECSEE Channel L_2 : (a) the spiral path curve, (b) the amplifier unit cell, (c) graphic plane unit deformation, (d) the angle relation in torsion, and (e) the ECSEE-produced sample cross section

Die and punch were assumed as rigid bodies, whereas the copper billet was considered to be a deformable one. The prepared copper bar was determined experimentally by compression test under the PWS-1000 universal testing machine at the room temperature of 25 °C and the strain rate of 0.01/s (Ref 5). Then, the experimental data of the stress–strain data were imported into the material flow stress database of DEFORM-3D V6.1 software. The yield function type was chosen with the von Mises setting, and hardening rule was supported with an isotropic model. The Young’s modulus, poisson’s ratio, thermal expansion, thermal conductivity, heat capacity, and emissivity were defined as the constant of 1.15×10^5 (MPa), 0.33, 1.76×10^{-5} (mm/(mm °C)), 43 (N/(s °C)), 3.42 (N/(mm² °C)), and 0.7. The billet in the simulation process was modeled with 37484 tetrahedral elements. Constant friction factor at the interface between the billet and the die was determined experimentally with the friction coefficient of 0.1. Automatic remeshing was used to account for large strains, and direct iteration method solver was implemented. More information regarding the details of setting the parameters is available in the literature (Ref 5).

3.3 Experimental Procedures

Pure copper prepared by annealing treatment was selected as the ECSEE experimental samples. The extrusion process was performed on the YA32-315-type hydraulic machine,

with an extrusion rate of 1 mm/s. The main structural parameters of the ECSEE die cavity were chosen as follows: $\varphi=120^\circ$, $m=1.55$, $L_1 = 7$ mm, $L_2 = 10$ mm, and $L_3 = 10$ mm (Ref 5). After a single-pass extrusion test, the samples were cut into 12 samples along the longitudinal section (see Fig. 3(b)).

The received samples were first mechanically polished and then electrolytically polished. Electro-polishing was carried out in 500 mL distilled water + 250 mL phosphoric acid at room temperature for 6-8 min at 4 V. An EBSD analysis test was conducted on a TOUANATA400-type field emission SEM. The PASS 5 software was used for data handling. In this study, the textures are represented in the TD-ND-ED reference system (see Fig. 3(b)). The normal direction (ND, perpendicular to the extrusion direction) and the extrusion direction (ED) are represented as X0 and Y0. As illustrated in Fig. 1(a), the extruded sample is distorted on the ED–ND plane during the ECSEE deformation in Channel L_2 .

The TEM samples were prepared in the following sequence: sectioning, manual grinding, punching (wafer with a diameter of 3 mm), grinding pits, and ion milling. TEM observation was conducted on a Tecnai G2 F30 high-resolution transmission electron microscope at the accelerating voltage of 300 kV. A series of positions were selected in the periphery regions of the received sample for recording the microstructure evolution (shown in Fig. 3(b)).

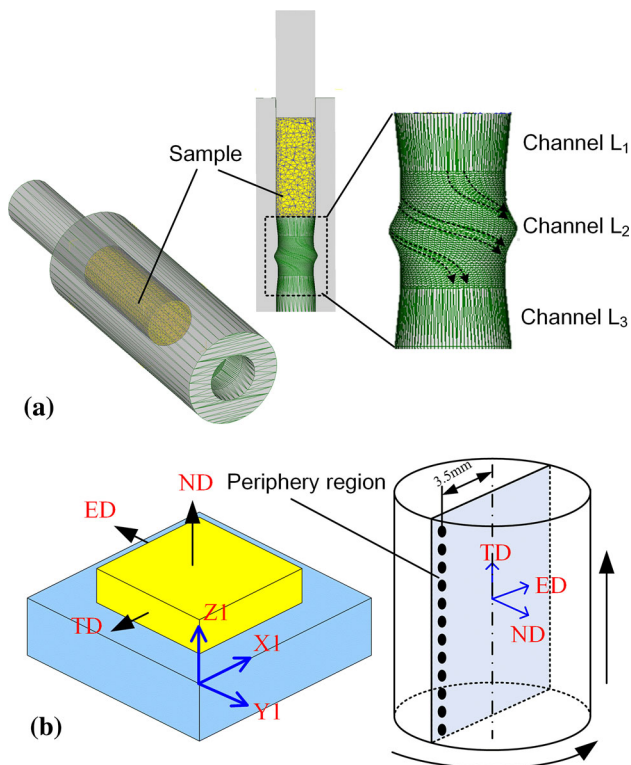


Fig. 3 (a) FEM model of ECSEE, and (b) the coordinate axis systems of samples and a crystal

Vickers micro-hardness tests were employed by using 100 g loads and a dwell time of 15 s with a HXP-1000TM micro-hardness tester. The micro-hardness measurements at 50 selected points were investigated along the lateral line and the central line of the longitudinal sections. For each selected point, three measurements were performed, and the average values were then used.

4. Results and Discussions

4.1 Simulation Analysis

Normally, the friction in the plastic deformation is detrimental to the billet forming process (Ref 12). However, it has something positive as far as blocking the material slide and controlling the deformation direction are concerned. The distribution of the average effective strain (AES) of the ECSEE-induced sample under different friction factors is shown in Fig. 4(a). With the friction factor increasing, the AES value increases, and the distribution is uniform. Consequently, the ECSEE method can reasonably make use of the friction in the course of plastic deformation. The harmful friction of torsional shear deformation is transformed into a driving force for the strain accumulation (Ref 3). The calculated results also show that the AES of ECSEE also increases with the increase in friction. It is known that strain accumulation can assist the large plastic deformation of materials. As shown in Fig. 4(a), the high friction factor corresponds to a high AES value. The friction factors of 0.7 and 0.08 correspond with the AES values of ~ 3 and ~ 2 , respectively. In addition, the analysis of AES distribution found that the higher the friction

factor is, the more even the strain distribution is. It is evident that in addition to increasing the strain, the friction increase can also improve the uniform degree of deformation. On the contrary, the friction is very detrimental to the practical engineering application. The analysis above shows that in the ECSEE deformation process, the increase in the friction factor is equivalent to the indirect increase in the effect of ECSEE torsional deformation. Oruganti et al. (Ref 13) noted that an appropriate increase in the friction coefficient could improve the deformation uniformity of the ECAP process.

The AES distribution of the ECSEE-induced samples for different ratios is shown in Fig. 4(b). In the case of low values of m , the deformation accumulation of AES as a whole is relatively low. In respect to the unified scale of AES (the bar label in the right figure), a significant strain change cannot be observed. With the increase in m , the deformation accumulation becomes more obvious. At the same time, the non-uniformity of the distribution becomes ever increasingly pronounced. Previous studies indicated that a large strain is generally focused on both ends of the major axis of the oval cross-sectional area and a relatively small one in the minor-axis region. The strain difference corresponding to the accumulation of major-axis and minor-axis regions will reduce with the value of m increasing. As shown in Fig. 4(b), for the low selected m values, the distribution of AES area is relatively narrow. With the increase in the m value, the distribution continues to the high-strain zone and exists in the shape form of low-slope valley. The deformation uniformity of $m = 1.3$ and 1.4 is higher than that of $m = 1.5$.

According to the analytical formula (4), it can be predicted that the AES of the ECSEE-induced copper is dramatically improved in the case of a large torsional angle. The obvious influence of the torsional angle on the deformation degree and deformation distribution uniformity can be easily seen (see Fig. 4(c)). Considering the elastic/plastic deformation characteristics, improvement in the strain distribution uniformity of the ECSEE-processed sample can be obtained by increasing the torsional angle. The increase in torsional angle is equivalent to the increasing torque of torsional deformation. As shown in Fig. 4(c), with the increase in torsional angle, the strain accumulation is significant, and the deformation uniformity can show very high enhancement. At a large torsional angle, the valley frontier slope of the strain distribution becomes relatively flat. Therefore, the increase in the torsional angle can improve not only the efficiency of billet deformation but also the uniformity of material deformation.

4.2 EBSD Analyses

The EBSD analysis of the ECSEE-induced sample is shown in Fig. 5. As shown in Fig. 5(a), the initial grains are stretched along the torsional shear, and some crushed grains become small grains with LAGBs. The white solid lines and the red solid lines denote LAGBs and HAGBs, respectively. As illustrated in the image quality of Fig. 5(a), the fine broken grains and/or subgrains approach the same orientation. The size of grains is slightly smaller than $4 \mu\text{m}$, and the fraction of the grains with a size smaller than $1 \mu\text{m}$ is above 50%. The misorientation analysis of grain boundaries shows that the proportion of HAGBs exhibits an obvious increasing trend with ECSEE (in Fig. 5(b)). However, the proportion of LAGBs is still high due to the use of only a single ECSEE deformation pass. The deformation of ECSEE-produced material is mainly

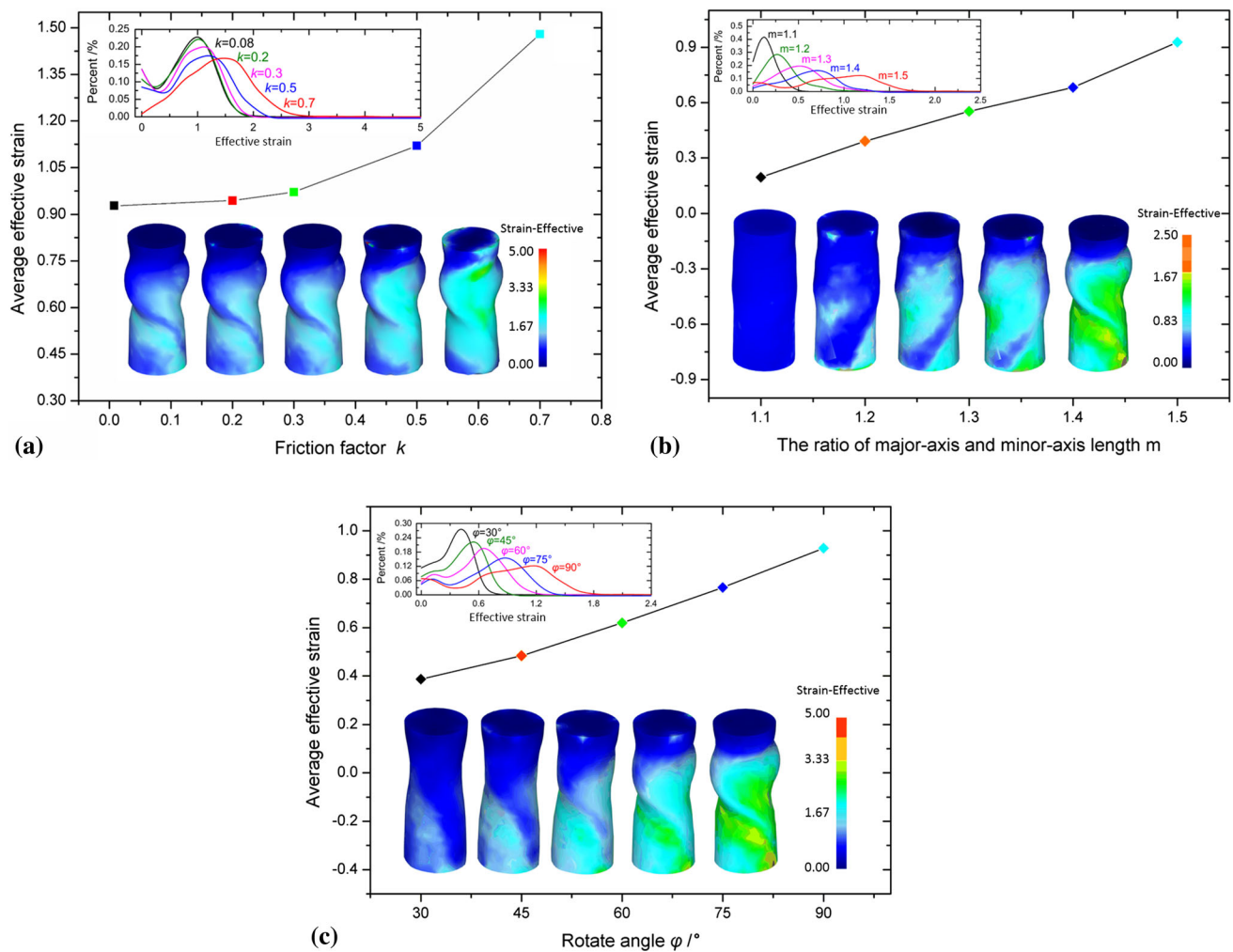


Fig. 4 Influence of (a) friction factor, (b) the ratio of major-axis and minor-axis lengths, and (c) torsional angle on the AES distribution

dominated by the torsional shear, and the macro-texture shows a visible change. The deformation grains are elongated and coordinated with each other toward a preferred orientation. Grains between each other show local changes with many subgrain boundaries emerging. As shown by optical microscopy (Ref 5), the grains are elongated along the shear direction. The grains show an obviously superior orientation, and the misorientation of the grain boundaries increases gradually with deformation increasing; the LAGBs are hereby replaced by the grain boundaries with larger angles. The deformation microstructure generally shares the same border with occurrence of the shear strain process (Ref 14). Under a low strain, a slip system arises in the polycrystal material. Increasingly more slip systems could operate with the increasing deformation. The different sets of slip systems lead to different lattice rotations for the coordination of the imposed strains. Moreover, the ECSEE deformation leads to the grain shear, accompanied by the increasing fraction of the substructure and misorientation. The increase in misorientations is located within the deformation bands and is due to the formation of new HAGBs (Ref 15, 16).

Material texture is defined as a microstructural property that describes the orientation distribution of the grains constituting a polycrystalline aggregate. The texture is most often related to plastic anisotropy, which depicts the dependence of the plastic

deformation response on the sense and direction of loading. For ECSEE, the textures would be similar to the simple shear textures of the shear-based torsion process. The most important ideal orientations in simple shear are distributed along the two fibers with a crystallographic slip direction parallel to the shear direction and a crystallographic slip plane parallel to the shear plane (Ref 17, 18).

As the $\{111\}$ pole figure of pure copper samples after a single pass of ECSEE deformation is shown in Fig. 5(e), a key for the locations of these ideal orientations and fibers is shown in Fig. 5(c). This appearance of texture is ascribed to the simple shear in a single pass of ECSEE deformation. Grains of deformed material form a strong texture orientation and present the non-symmetry pole. The strong simple shear texture is well developed in the peripheral region of the one-pass ECSEE-deformed sample (Fig. 5(e)). As it can be expected from the transformation from the $x'y'z$ to the xyz reference system, the texture is rotated counterclockwise (CCW rotated) by $\theta = \Phi/2 = 45^\circ$ around the TD direction from the shear texture. Accordingly, the main texture components and fibers in the texture are CCW rotated. The main components can be denoted as TD rotated (CCW 45°). An orientation along the $\langle 110 \rangle$ -fiber has a $\langle 110 \rangle$ -direction rotated counterclockwise by θ from the ED direction, and an orientation along the $\{111\}$ -plane CCW rotated by θ from the ED-ND

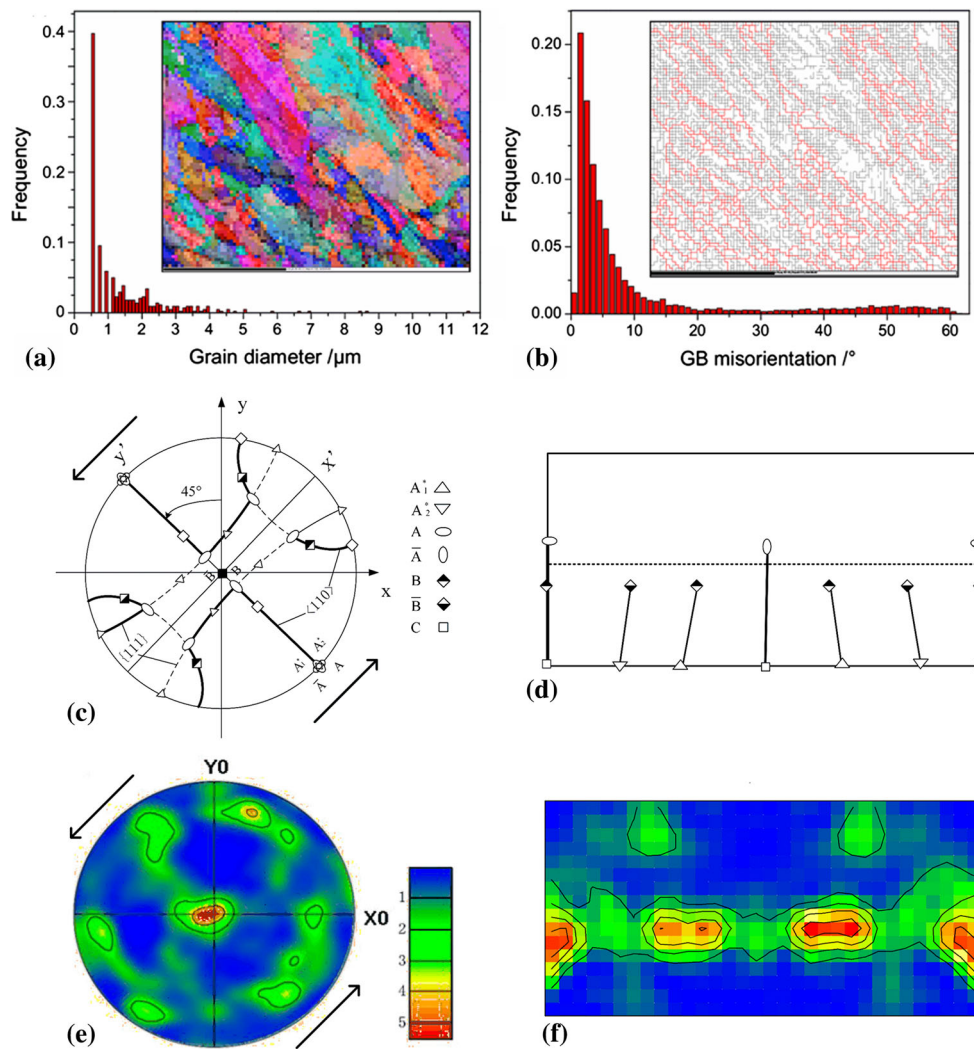


Fig. 5 (a) Grain OIM maps and grain size distributions, (b) grain boundary restructuring graph and misorientation, (c) (110) end texture pole figures depicting simple shear orientations and partial fibers (solid lines) for fcc materials after one pass of ECSE with $\Phi = 90^\circ$ (Ref 21), (d) $\phi_2 = 45^\circ$ ODF sections of textures for fcc materials after the main ideal orientations in simple shear (Ref 21), (e) {111} pole figure, and (f) ODFs of pure copper deformed by one pass of the ECSE process

plane. The ECAP-specific orientations can also be derived from increasing the ϕ_1 of the ideal simple shear orientations by $\theta = 45^\circ$ while the other two Euler angles (ϕ and ϕ_2) remain constant (Ref 19). Development of ECAP textures can be drawn by the ideal orientations associated with simple shear (Ref 20).

Since ECSE is a shear-based process, it is beneficial to analyzing the orientation distribution function (ODF) sections in respect of the ideal orientations established for simple shear (Fig. 5(d)) (Ref 21). Ideal orientations in simple shear and their development were exhaustively attributed to torsion. For the construction of the ODFs of single-pass textures in copper for comparison with ideal shear orientations, the ODFs are referenced to the simple shear frame. Only the $\phi_2=45^\circ$ ODF section diagram of pure copper after the ECSE deformation for all major ideal orientations of shear textures is shown in Fig. 5(f). The ODF of the initial microstructure is omitted in the previous studies (Ref 19, 21). After a single pass of ECSE, the texture shows shear texture components. Nevertheless, some major changes are observed. The general texture intensity is reduced. The major component is the rotated cube, resulting in

the introduction of shear texture. The textures include the cube texture ($\{001\} \langle 100 \rangle$) and rotated cube texture ($\{001\} \langle 110 \rangle$). Such an unusual texture development may be related to the formation mechanism and the deformation mechanism of UFGs during the ECSE process.

4.3 Microstructure Evolution in TEM Observations

According to the TEM images of copper processed by a single pass of ECSE deformation, the process of grain refinement is divided into the following four stages shown in Fig. 6.

Stage I the initial coarse grains of pure copper are stretched into a thin shear strip morphology along the slip direction under the ECSE deformation (in Stage I(a) and Stage I(b)). The dense black lines along a certain direction appear in the interior grain. It is difficult for the cross slip to occur during these stages of the ECSE process. As a result, dislocation migration is difficult, and dislocations are retained in the short stacking slip bands. Therefore, a large number of slip bands emerge. With the deformation intensifying, slip bands tend to be dense,

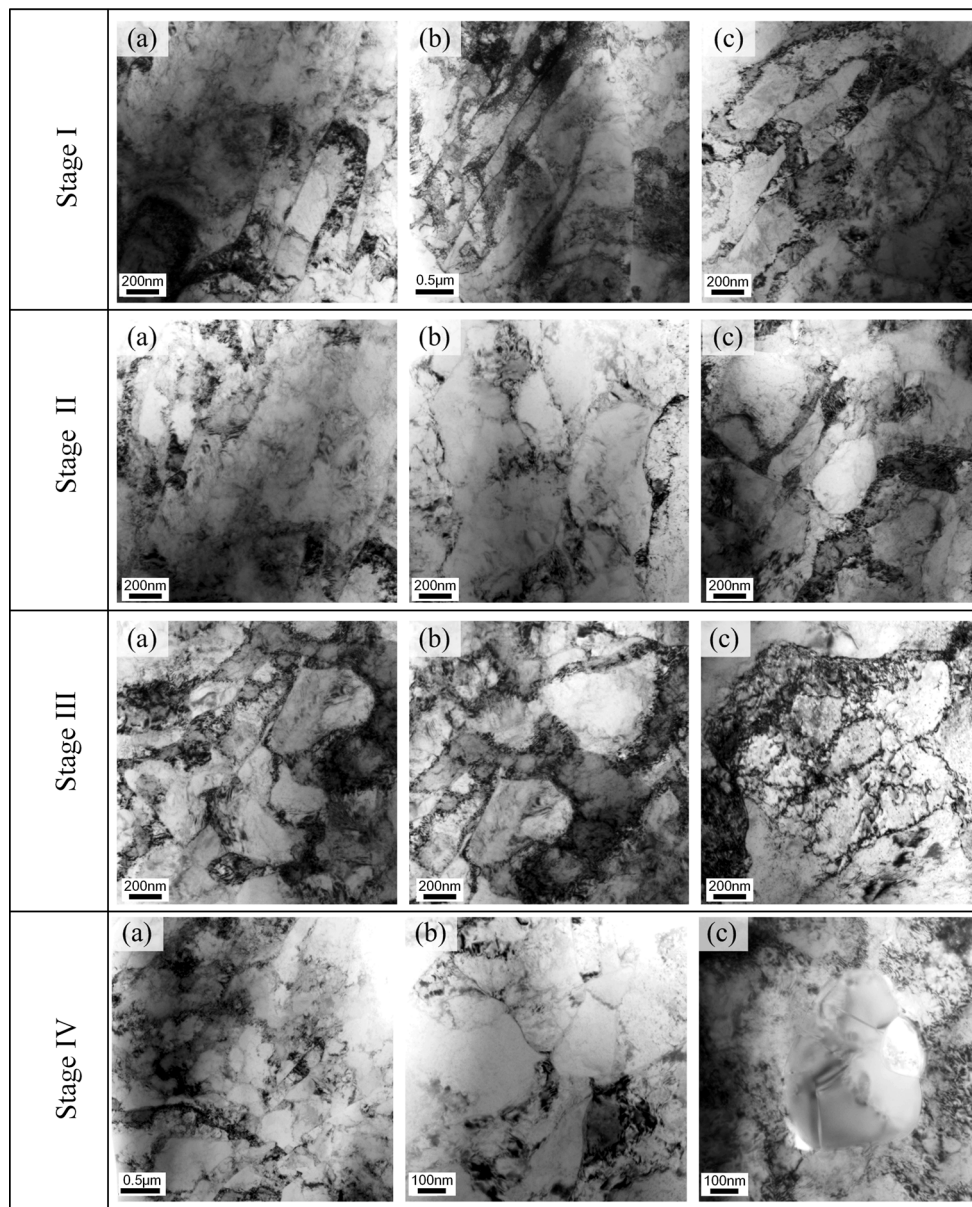


Fig. 6 TEM micrographs (bright field) of stage I, stage II, stage III, and stage IV for one pass of ECSEE-processed copper: (a) early; (b) middle; and (c) end

and the directions are consistent with the shear direction. When the strain accumulates to a certain degree, the shear zone shows an anisotropic microstructure distribution in general. According to Ref 22, 23, the shear zone can be divided into two categories: the deformation zone and the transition zone. The former consists of a large number of strain localizations, and future deformation will generate the transition zone. As shown in Stage I in Fig. 6, the shear zone is mainly the deformation zone due to the low degree of ECSEE deformation. With the deformation proceeding, the grain is fully extended along the shear direction, forming a zigzag and partial crushing grain. The initial grain boundary is not observed clearly. It exhibits short fibrous tissue morphology as well as a large number of dislocations gathered on the boundary (Stage I-c in Fig. 6). The shear zone accompanies with the localization of inhomogeneous deformation, and thus, in the shear zone, a large number of strains are accumulated and surrounded by high-density

dislocation tangles (Ref 24). The shear zone can coordinate the deformation harmony and reasonable strain distribution by consuming the deformation energy of the slip and recovery. Once a certain critical value is exceeded, the shear zones will initiate micro-cracks (Ref 25). This is the reason for the increasing three-direction hydrostatic pressure for the material under the SPD process.

Stage II The lath-shaped microstructure increases, and crushing and slip appear with the increase in the deformation (Stage II-b to Stage II-c in Fig. 6). The joggling phenomenon appears on the broken crystal in the resulting dislocation cluster. In addition, a certain amount of slip systems is required to start the formation of a low-energy dislocation structure. The small slip system start will make the deformation coordination difficult. However, if the running number of slip system were much too high, the number of jogs on the dislocation intersection would increase. Therefore, the deformation resis-

tance of the material will increase within a certain threshold. The reasonable number of initiated slip systems is 3-5 in each region.

Stage III This is the initial formation stage for the dislocation cell of a broken crystal. The dislocation in Stage III-a is not obvious (seen in Fig. 6). Which in turn, the shear zone is elongated along the shear direction. As the deformation continues, the grains are fragmented by the different running numbers of slip systems in each region. For the overall coordination deformation of the grain, the region after the “fragmentation” is separated by the transition zone and/or dense dislocation wall. The separating boundary is called the geometrically necessary boundary. Comparison of Stage III-c with Stage III-b shows that the dislocation aggregation changed strongly with the increase in the strain.

Stage IV This stage is the mature formation period of the dislocation cell (see Stage IV in Fig. 6). The deformed material microstructure is mainly made up of cellblocks and diffuse cell walls. The formations contain a high density of dislocation tangles. However, the intragranular dislocation density is quite low at this stage. The dislocation mechanism is expected to explain the phenomenon above in the process of metal material deformation. The dislocation appears in the high-density cluster configuration, which is consistent with the interaction during the deformation process of metal materials. These configurations are dislocation tangles, two-dimensional dislocation walls, and three-dimensional approximation equiaxed dislocations. This cell structure can produce microstructure relaxation through dislocation movement. This is a natural way of releasing the energy. The random distribution of the dislocation cluster could be a result of the recovery process in the deformed material. Dislocation clusters can greatly reduce the interaction between the dislocations and lead to a greatly reduced long-range stress field because of their mutual shielding. It is suggested that increasing the Burgers vector of cluster dislocation can not only make stress shielding more effective but also decrease the micro-misorientation between the dislocations. Therefore, the cluster dislocation is a type of low-energy dislocation structure. The thickness of the dislocation cell wall was increased during the deformation process (Stage IV in Fig. 6).

Previous studies stated that the grain refinement of SPD-induced material showed contributions from dislocation gliding, accumulation, interaction, tangling, and spatial rearrangement. Numerous models described these deformation modes (Ref 26, 27). Among these, Taylor’s model is the most appropriate for the formation of equiaxed grains. Similar to Taylor’s model (Ref 26), the majority of material grain orientations have changed, and the grain shape is elongated in a single pass of ECSEE deformation. The elongated laminar structures form along the main slip plane under the shear deformation. With the increase in the deformation, random dislocations are generated in the initial grain boundary and the internal grain without any organized structure. These cell patterns constitute isotropic dislocation. To coordinate this deformation, cell walls sequentially coalesce and straighten, and self-organized gliding along active slip planes will be initiated (Ref 28). Gliding of dislocation groups annihilates or untangles dislocations from the initial cell walls, causing the cell wall boundaries to become thinner. Finally, the formation of large-angle equiaxed grains is completed with the coordination of the plastic deformation.

4.4 Hardness Measurements

Micro-hardness distribution along the central line and lateral line on the longitudinal section of the deformed sample is presented in Fig. 7(a), and the corresponding variation curves of hardness value are shown in Fig. 7(b). The black and red curves represent the hardness of selected points along the lateral and central lines, respectively. In early studies, completely annealed copper was discovered to show a relatively uniform hardness distribution with an initial mean hardness of ~ 40 Hv, significantly lower than that of the ECSEE-deformed samples (Ref 4, 5). The annealing process could eliminate the anisotropy of samples. It can be seen that the value of the marginal area is higher than that of the center due to the uneven deformation of ECSEE. Similar to the pure torsion, the stress and strain are transmitted from the surface to the interior in the bar sample. An inconsistency is always present between the center and the circumference due to the geometrical feature of the deformation. Similar phenomena also emerged in HPT (Ref 29) and TE (Ref 30). This is consistent with the evolution of torsion properties. Both curves are divided into four segments corresponding to the ECSEE formation sections (see Fig. 7(b)). In Segment I, the central line is slightly higher than the lateral line. In Segment II, the central line overlaps with the lateral line. Nevertheless, a careful examination shows that the red line is slightly higher. For the above two segments, the hardness variation is relatively smooth of the material deformation, mainly in Channel L_1 of the ECSEE die. The stretching deformation mode is dominant over the core axis pulling of the sample. Hence, the influence of the central hardness is is

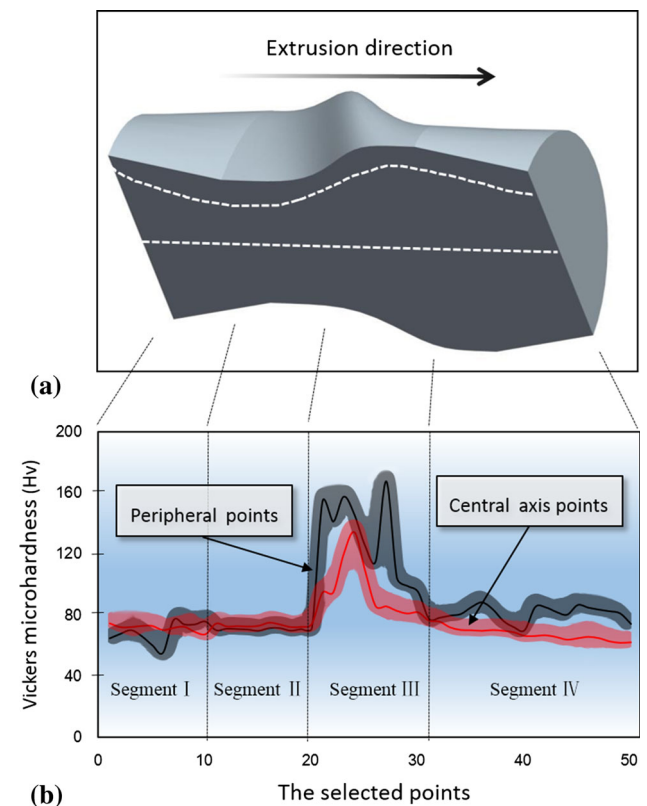


Fig. 7 (a) Hardness measurement position and (b) hardness variation on the longitudinal section

relatively obvious. In Segment III, the lateral line jumps up and shows a severe periodic fluctuation. On the other hand, the jitter of the central line is relatively mild due to the low strain. The deformation in Channel L_2 of the ECSEE die for the sample propagates the simple shear strain, refining the material grain, especially the surface part of the bar sample. In Segment IV, both curves decrease to the smooth linear state. The periodicity of fluctuation becomes less pronounced, qualitatively indicating a continuous improvement in deformation inhomogeneity. The black curve is higher than the red curve for the deformation non-uniformity. Experimental error is presented in the downward trend for the central area measurement. This segment corresponds to the deformation in Channel L_3 of the ECSEE die. The above phenomenon indeed reveals the intrinsic links between the effective strain and micro-hardness (Ref 31).

5. Conclusions

1. The strain distribution feature of the ECSEE-induced sample is much more associated with the following parameters: the torsional angle, friction factor, and ratio of elliptical cross section. A high value of the above parameters can improve both the AES accumulation and the distribution uniformity.
2. The non-uniform shear deformation is dominant in the process of single pass of ECSEE. The microstructure of the shear band with LAGBs transforms into more subgrains with HAGBs along the torsional shear direction. The obvious misorientation of grain boundaries adds up with the increase in the ECSEE deformation.
3. The texture of the ECSEE-induced pure copper is rotated counterclockwise by $\theta = \Phi/2 = 45^\circ$ around the TD direction from the shear texture. The strong shear texture of the rotated cube, including the cube texture ($\{001\} <100>$) and rotated cube texture ($\{001\} <110>$), is stimulated with the ECSEE deformation.
4. The grain refinement process of deformed copper shows the following sequence: (I) The initial coarse grains are stretched into a lath-like microstructure with a high dislocation density under the effect of shear strain. (II) Dislocation walls or cells with small-angle boundaries appear. (III) The small subgrains transform into equiaxed grains with HAGBs through orientation rotation and shear absorption.
5. Compared to the as-annealed sample, the hardness values of ECSEE-processed samples are significantly improved. The hardness distribution features are consistent with both the deformation characteristics and the strain distribution.

Acknowledgments

This work was supported by National Natural Science Foundation of China (No. 51275414, 51172161) and the fund of the State Key Laboratory of Solidification Processing in NWPU (No. SKLSP201517).

References

1. R.Z. Valiev and A.K. Mukherjee, Nanostructures and Unique Properties in Intermetallics, Subjected to Severe Plastic Deformation, *Scr. Mater.*, 2001, **44**, p 1747–1750
2. C.P. Wang, F.G. Li, W. Lei, and H.J. Qiao, Review on Modified and Novel Techniques of Severe Plastic Deformation, *Sci. China Technol. Sci.*, 2012, **55**, p 2377–2390
3. C.P. Wang, F.G. Li, B. Chen, Z.W. Yuan, and H.Y. Lu, Severe Plastic Deformation Techniques for Bulk Ultrafine-Grained Materials, *Rare Metal. Mater. Eng.*, 2012, **41**, p 941–946
4. C.P. Wang, F.G. Li, Q.H. Li, L. Wang, and J.Z. Dong, A Novel Severe Plastic Deformation Method for Fabricating Ultrafine Grained Pure Copper, *Mater. Des.*, 2013, **43**, p 492–498
5. C.P. Wang, F.G. Li, Q.H. Li, and L. Wang, Numerical and Experimental Studies of Pure Copper Processed by a New Severe Plastic Deformation Method, *Mater. Sci. Eng. A*, 2012, **548**, p 19–26
6. J.H. Li, F.G. Li, C. Zhao, H. Chen, X.K. Ma, and J. Li, Experimental Study on Pure Copper Subjected to Different Severe Plastic Deformation Modes, *Mater. Sci. Eng. A*, 2016, **656**, p 142–150
7. J.H. Li, F.G. Li, X.K. Ma, H. Chen, Z.C. Ma, and J. Li, Microhardness Distribution and Microstructural Evolution in Pure Aluminum Subjected to Severe Plastic Deformation: Elliptical Cross-Sectioned Spiral Equal-Channel Extrusion (ECSEE), *J. Mater. Eng. Perform.*, 2015, **24**, p 4543–4550
8. C.P. Wang, F.G. Li, H.Y. Lu, Z.W. Yuan, and B. Chen, Optimization of Structural Parameters for Elliptical Cross-Section Spiral Equal-Channel Extrusion Dies Based on Grey Theory, *Chin. J. Aeronaut.*, 2013, **26**, p 209–216
9. C.P. Wang, F.G. Li, H.Y. Lu, Z.W. Yuan, B. Chen, and H.J. Qiao, Deformation Analysis of Elliptical Cross-Section Spiral Equal Channel Extrusion Technique, *Rare Metal. Mater. Eng.*, 2013, **42**, p 679–683
10. R.E. Bolmaro and U.F. Kocks, A Comparison of the Texture Development in Pure and Simple Shear and During Path Changes, *Scr. Metal. Mater.*, 1992, **27**, p 1717–1722
11. V.M. Segal, Severe plastic Deformation: Simple Shear Versus Pure Shear, *Mater. Sci. Eng. A*, 2002, **338**, p 331–344
12. W.R.D. Wilson, Friction and Lubrication in Bulk Metal-Forming Processes, *J. Appl. Metalwork.*, 1978, **1**, p 7–19
13. R.K. Oruganti, P.R. Subramanian, J.S. Marte, M.F. Gigliotti, and S. Amancherla, Effect of Friction, Backpressure and Strain Rate Sensitivity on Material Flow During Equal Channel Angular Extrusion, *Mater. Sci. Eng. A*, 2005, **406**, p 102–109
14. F. Salimyanfard, M.R. Toroghinejad, F. Ashrafzadeh, and M. Jafari, EBSD Analysis of Nano-Structured Copper Processed by ECAP, *Mater. Sci. Eng. A*, 2011, **528**, p 5348–5355
15. W. Skrotzki, N. Scheerbaum, C.G. Oertel, R. Arruffat-Massion, S. Suwas, and L.S. Tóth, Microstructure and Texture Gradient in Copper Deformed by Equal Channel Angular Pressing, *Acta Mater.*, 2007, **55**, p 2013–2024
16. S.R. Bahadori, K. Dehghani, and F. Bakhshandeh, Microstructure, Texture and Mechanical Properties of Pure Copper Processed by ECAP and Subsequent Cold Rolling, *Mater. Sci. Eng. A*, 2013, **583**, p 36–42
17. S. Li, I.J. Beyerlein, C.T. Necker, D.J. Alexander, and M. Bourke, Heterogeneity of Deformation Texture in Equal Channel Angular Extrusion of Copper, *Acta Mater.*, 2004, **52**, p 4859–4875
18. M. Shaarbaq and M.R. Toroghinejad, Evaluation of Texture and Grain Size of Nanograined Copper Produced by the Accumulative Roll Bonding Process, *Metall. Mater. Trans. A*, 2009, **40**, p 1693–1700
19. S. Ferrasse, V.M. Segal, S.R. Kalidindi, and F. Alford, Texture evolution During Equal Channel Angular Extrusion: Part I. Effect of Route, Number of Passes and Initial Texture, *Mater. Sci. Eng. A*, 2004, **368**, p 28–40
20. S. Li, I.J. Beyerlein, D.J. Alexander, and S.C. Vogel, Texture Evolution During Equal Channel Angular Extrusion: Effect of Initial Texture from Experiment and Simulation, *Scr. Mater.*, 2005, **52**, p 1099–1104
21. S. Li, I.J. Beyerlein, and M.A. Bourke, Texture Formation During Equal Channel Angular Extrusion of fcc and bcc Materials: Comparison with Simple Shear, *Mater. Sci. Eng. A*, 2005, **394**, p 66–77
22. L. Zhen, D.L. Zou, C.Y. Xu, and W.Z. Shao, Microstructure Evolution of Adiabatic Shear Bands in AM60B Magnesium Alloy Under Ballistic Impact, *Mater. Sci. Eng. A*, 2010, **527**, p 5728–5733

23. D.L. Zou, L. Zhen, C.Y. Xu, and W.Z. Shao, Characterization of Adiabatic Shear Bands in AM60B Magnesium Alloy Under Ballistic Impact, *Mater. Character.*, 2011, **62**, p 496–502
24. S.M. Fatemi-Varzaneh, A. Zarei-Hanzaki, and J.M. Cabrera, Shear Banding Phenomenon During Severe Plastic Deformation of an AZ31 Magnesium Alloy, *J. Alloy. Compd.*, 2011, **509**, p 3806–3810
25. A.G. Beer and M.R. Barnett, Microstructural Development During Hot Working of Mg-3Al-1Zn, *Metall. Mater. Trans. A*, 2007, **38**, p 1856–1867
26. J.Y. Huang, Y.T. Zhu, H. Jiang, and T.C. Lowe, Microstructures and Dislocation Configurations in Nanostructured Cu Processed by Repetitive Corrugation and Straightening, *Acta Mater.*, 2001, **49**, p 1497–1505
27. R.Z. Valiev, Y.V. Ivanisenko, E.F. Rauch, and B. Baudalet, Structure and Deformation Behaviour of Armco Iron Subjected to Severe Plastic Deformation, *Acta Mater.*, 1996, **44**, p 4705–4712
28. Q. Xue, I.J. Beyerlein, D.J. Alexander, and G.T. Gray, Mechanisms for Initial Grain Refinement in OFHC Copper During Equal Channel Angular Pressing, *Acta Mater.*, 2007, **55**, p 655–668
29. C. Xu, Z. Horita, and T.G. Langdon, The Evolution of Homogeneity in Processing by High-Pressure Torsion, *Acta Mater.*, 2007, **55**, p 203–212
30. S.A. Mousavi and S.R. Bahadori, The Effects of Post Annealing on the Mechanical Properties, Microstructure and Texture Evolutions of Pure Copper Deformed by Twist Extrusion Process, *Mater. Sci. Eng. A*, 2011, **528**, p 1242–1246
31. X.P. Mou, K.P. Peng, J.W. Zeng, L.L. Shaw, and K.W. Qian, The Influence of the Equivalent Strain on the Microstructure and Hardness of H62 Brass Subjected to Multi-Cycle Constrained Groove Pressing, *J. Mater. Process Technol.*, 2011, **211**, p 590–596